John G. Michopoulos
Naval Research Laboratory,
Center of Computational Material Science,
Computational Multiphysics Systems Laboratory,
Washington, DC 20375

John C. Hermanson
USDA Forest Service,
Forest Products Laboratory,
Engineering Properties of Wood, Wood Based
Materials, and Structures,
Madison, WI 53726

Athanasios Iliopoulos
Science Applications Int. Corp.
Resident at Naval Research Laboratory,
Center of Computational Material Science,
Computational Multiphysics Systems Laboratory,
Washington DC 20375

Samuel G. Lambrakos
Naval Research Laboratory,
Center of Computational Material Science,
Computational Multiphysics Systems Laboratory,
Washington DC 20375

Tomonari Furukawa
Virginia Polytechnic Institute and State
University,
Department of Mechanical Engineering,
Computational Multiphysics Systems Laboratory,
Danville, VA 24540

Data-Driven Design Optimization for Composite Material Characterization

The main goal of the present paper is to demonstrate the value of design optimization beyond its use for structural shape determination in the realm of the constitutive characterization of anisotropic material systems such as polymer matrix composites with or without damage. The approaches discussed are based on the availability of massive experimental data representing the excitation and response behavior of specimens tested by automated mechatronic material testing systems capable of applying multiaxial loading. Material constitutive characterization is achieved by minimizing the difference between experimentally measured and analytically computed system responses as described by surface strain and strain energy density fields. Small and large strain formulations based on additive strain energy density decompositions are introduced and utilized for constructing the necessary objective functions and their subsequent minimization. Numerical examples based on both synthetic (for one-dimensional systems) and actual data (for realistic 3D material systems) demonstrate the successful application of design optimization for constitutive characterization. [DOI: 10.1115/1.3595561]

Keywords: design optimization, material characterization, mechatronic systems, constitutive response, anisotropic materials, polymer matrix composites, multiaxial testing, full-field methods

Introduction

Design optimization, as a topic of research relative to engineering applications and product development has been popular within the context of optimal shape determination but not as popular within the context of material characterization. In an attempt to fill this gap, the main objective of the present paper is to describe design optimization efforts in the less popular application area of the data-driven constitutive characterization of anisotropic material systems. In this context, the term "design optimization" refers to the material constitutive model as being the "under design" entity, in contrast to the traditionally considered "shape model" where the target design entity is that of the "shape model." Formally, however, this is again an application optimization for solving the inverse problem of identifying material model parameters when experimental data describing the systemic behavior are known.

Composite materials are clearly the most widely used anisotropic materials for various application areas [1,2]. Their constitutive characterization has been an important topic of interest for structural design, material certification, and qualification practitioners. Such characterization has been traditionally achieved through mostly uniaxial tests aiming in the determination of elastic material properties primarily. Typically, extraction of these properties, involve uniaxial tests conducted with specimens mounted on uniaxial testing machines, where the major orthotropic axis of any given specimen is inclined relative to the loading direction. In addition, specimens are designed such that a homogeneous state of strain is developed over preferably a large and well-defined area of the specimen, such that the measurement of specimen loads and displacements [3,4] can be reduced to material field quantities such as stresses and strains. Consequently, the use of uniaxial testing machines imposes requirements of using multiple specimens, gripping fixtures, and multiple experiments. The requirement of a homogeneous state of strain frequently imposes restrictions on the size and shape of specimens to be tested. It follows that these requirements result in increased cost and time, and consequently to inefficient characterization processes.

To address these issues and to extend characterization to nonlinear regimes of the constitutive behavior, multi-degree of freedom automated mechatronic testing machines, were introduced at the Naval Research Laboratory (NRL) [5–7] in order to enable the capability of loading specimens multiaxially in conjunction with the employment of energy-based inverse characterization methodologies. This introduction was the first of its kind and has continued through the present [8–10]. The most recent prototype of these machines, which is currently under functional verification [11], is shown in Fig. 1.

The energy-based approach associated with mechatronic testing, although it enables multiaxial loading and inhomogeneous states of strain, still requires multiple specimens. It is significant to state, however, that these specimens are tested in an automated manner with high throughput that has reached values of 30 specimens per hour.

The recent development of flexible full-field displacement and strain measurements methods has afforded the opportunity of alternative characterization methodologies [12–15]. Full-field optical techniques, such as Moire and Speckle Interferometry, digital image correlation, and meshless random grid method (MRGM), which measure displacement and strain fields during mechanical tests, have been used mostly for elastic characterization of various

Contributed by the CAD/Solid Modeling Committee of ASME for publication in the Journal of Computing and Information Science in Engineering. Manuscript received October 29, 2010; final manuscript received April 12, 2011; published online June 22, 2011. Assoc. Editor: J. Shah.

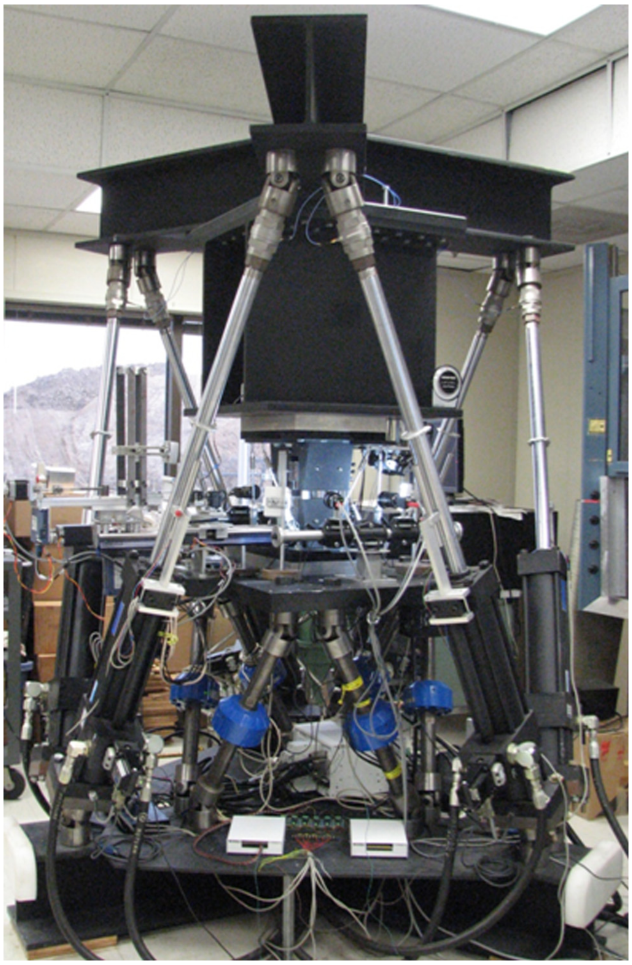

Fig. 1 NRL66.3: Most recent 6-DoF mechatronically automated system for the multiaxial testing of materials

materials [15–18]. The resulting measurements are used for identification of constitutive model constants, via the solution of an appropriately formed inverse problem, with the help of various computational techniques.

Arguably, the most popular methodology is the mixed numerical/experimental method that identifies the material's elastic constants by minimizing an objective function formed by the difference between the full-experimental measurements and the corresponding analytical model predictions via an optimization method [5–10,15,17–20]. However, the repetitive finite element analysis (FEA) required for each iteration of the optimization process makes the computation considerably costly [21]. Alternatively, the so-called virtual field method was developed [21–23] to identify material parameters by finding virtual fields and inversely solving for parameters by substitution of full-field/surface measurements. That is to say, the virtual field method effectively characterizes materials without finite element analysis, provided that appropriate virtual fields are derivable.

Our focus in the present work is to describe our recent efforts concerning design optimization methodologies for constitutive material characterization. Our approaches are based mostly on energy conservation arguments, and they can be classified according to computational cost in relation to whether FEA are used iteratively inside the optimization loop or not. It is important to clarify that digitally acquired images are processed by in-house developed software that implements the MRGM [24,27,28] and is used to measure the full-field displacement and compute the associated strain fields as well as the boundary displacements required for material characterization. Reaction forces and redundant boundary displacement data are acquired from displacement and force sensors integrated with NRL's multiaxial loader—called NRL66.3—[11]. In an effort to address the computational cost of the FEA-in-the-loop approaches, the authors have initiated a dissipated and total strain energy density determination approach [29–32] that has recently been extended to a framework that is derived from the total potential energy and the energy conservation, which can be applied directly with full field strain measurement for characterization [33,34].

Two techniques, built upon this framework, have been proposed to identify elastic constants and to develop nonparametric constitutive models of anisotropic materials.

The first identification technique estimates the elastic constants for every set of measurements by equating the variation of the external work, derived from the boundary displacement/force measurements, with that of the induced strain energy, derived from the full-field strain measurements, and stochastically correcting the estimation using a Kalman filter approach [34]. This technique has been proven to identify the elastic constants of anisotropic materials even under the presence of considerable noise in the measurements [34].

The second technique develops nonparametric representations of constitutive models using artificial neural networks [35]. When we first explored this approach in the early nineties [36], we determined that the computational performance of the approach, as it was implemented on the Aspirin/MIGRAINES neural net simulator framework [37], was not practical for the amounts of data generated by NRL's multidimensional testing machines. Subsequently, we have applied it on many other material characterization applications [38–42] for less amounts of data where it was practical. In these efforts, the error between the energy quantities is used to develop the neural network constitutive model, unlike the conventional techniques where stress data are required for the modeling [43–46]. This technique allows the nonlinear constitutive relations to be modeled comprehensively without the limitations imposed by the parametric expressions of the conventional material models. Since both artificial neural network (ANN) implementations and full field measurement techniques have matured, we have decided to apply ANN technologies for material characterization of the damage behavior of composite materials [47]. It should be noted that some efforts for characterizing nonlayered anisotropic biological materials like trabecular bone have been implemented using FEA in the context of numerical experiments and without the use of experimental measurements [48].

In order to maintain reasonable scope, this paper considers only methodologies that require FEA-in-the-loop because of the simplicity of their implementation and exhaustive capability to determine the material parameters. The consideration of other methodologies is more appropriate for future comparative studies.

In the section that follows, we will present the general case of material characterization from a systemic perspective in order to establish a common reference. Next, we present the case of determining the properties of the one-dimensional nonlinear system. This is done mainly for instructive purposes, which bare relevance to subtleties of subsequent formulations presented. Next, we present a small strain formulation (SSF) of the general strain energy density approach followed by a finite strain formulation (FSF), which is for the case of linear and nonlinear constitutive behavior of composite materials with or without damage. The paper continues with a numerical application of design optimization implementations based on these two formulations, which are in turn based on both synthetic and actual data. Finally, conclusions are presented.

General System Representation for Material Characterization

For the general case of a material system, there are two representations (see Fig. 2.) The actual physical system and the analytical model representation of the system whose general functional form is

$$\mathbf{y} = f(\mathbf{p}; \mathbf{x}) \tag{1}$$

where $\mathbf{y} \in Y^{q_y} \subseteq \mathbb{R}^{q_y}$ and $\mathbf{x} \in X^{q_x} \subseteq \mathbb{R}^{q_x}$ represent q_y output and q_x input state variables, respectively. The vector $\mathbf{p} \in P^p \subseteq \mathbb{R}^p$ represents p unknown parameters characterizing the system (i.e., design variables within a design optimization context). The vector function $f(\mathbf{p}; \mathbf{x}) \in Y^{q_y} \subseteq \mathbb{R}^{q_y}$ represents the behavior of the system.

Determination of this vector function is equivalent to a determination of all q_y components y_u of the vector $\mathbf{y}$. This is equivalent to the identification of q_y systems $y_u = f_u(\mathbf{p}; \mathbf{x})$. Assuming that one exercises the corresponding physical system l times, incrementally, one is then able to construct the experimental pairs $(y_u, \mathbf{x})_k^{\mathrm{E}} = (y_{u,k}^{\mathrm{E}}, \mathbf{x}_k^{\mathrm{E}})$, where $k = 1, \ldots, l$ and the superscript "E" indicates the experimental character of a given quantity. The experimental data are acquired by the utilization of an experimental frame that exercises physically the actual material system (i.e., a specimen loaded by a testing machine). It can also exercise the analytical material model computationally by presenting an optimizer with both the experimentally acquired systemic behavior as well as the computationally predicted model behavior. The model or the final material parameters emerge when the comparison by the optimizer between actual physical behavior and that predicted by analytical model are close to each other, within an acceptable margin.

At this stage, without loss of generality, it is advantageous to construct a multiplicative decomposition of $f_u(\mathbf{p}; \mathbf{x})$. This can be achieved in general using a formalism that is in terms of a Taylor-series expansion [49] according to

$$f_u(\mathbf{p}; \mathbf{x}) = \sum_{\mathbf{m}} p_u[\mathbf{m}] x_1^{m_1} x_2^{m_2} \ldots x_{q_x}^{m_m}. \tag{2}$$

The index vector $\mathbf{m} = [m_1, m_2, \ldots, m_m]$ is an m-tuple of nonnegative integers, which identifies the term in the series or equivalently, the order of each variable in each of the monomial terms of the series. This implies that the order of each monomial term is $m = |\mathbf{m}| = m_1 + m_2 + \cdots + m_m$. Thus, the number of terms in the series is given by the binomial coefficient

$$p_{up} = \binom{m + q_x}{m} \tag{3}$$

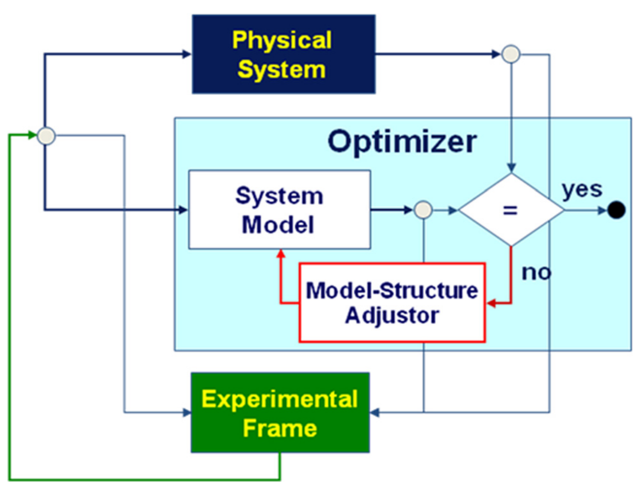

Fig. 2 Systemic outline of design optimization for constitutive material characterization

which defines the dimensionality of the column parameter vector $\mathbf{p}$. The components of this vector or the coefficients of the series in Eq. (2) can now be considered as design variables of an optimization problem that requires minimization of the quantity $\|\mathbf{A}_u \mathbf{p}_u - \mathbf{b}_u\|$, which expresses the error between the experimentally observed output behavior $\mathbf{b}_u$ and that which is estimated analytically as expressed by the product $\mathbf{A}_u \mathbf{p}_u$. Here, $\mathbf{b}_u^T = (y_{u1}, \ldots, y_{uk}, \ldots, y_{ul})$, and $\mathbf{A}_u$ is an $l \times p_{up}$ array whose elements are evaluations of the combinations $x_1^{m_1} x_2^{m_2} \ldots x_{q_x}^{m_m}$ of terms from the series given in Eq. (2). When this minimization is defined with respect to the L_2 norm, one is able to construct [50] an objective function for minimization that is of the form

$$\begin{aligned} \left\|\mathbf{A}_u \mathbf{p}_u - \mathbf{y}_u^E\right\|_{L_2}^2 &= (\mathbf{A}_u \mathbf{p}_u - \mathbf{y}_u^E)^T (\mathbf{A}_u \mathbf{p}_u - \mathbf{y}_u^E) \\ &= \sum_{k=1}^{l} (\mathbf{A}_{uk} \mathbf{p}_u - \mathbf{y}_{uk}^E)^2 \end{aligned} \tag{4}$$

This formulation suggests that linear least squares methods can be used to determine the vector of the system parameters $\mathbf{p}_u$ that represent the coefficients of the generally nonlinear system model with respect of the input vector $\mathbf{x}$. This fact has generated confusion within the literature and therefore requires some emphasis for purposes of clarity. Consequently, $f(\mathbf{p}; \mathbf{x})$ can be determined through a determination of its components $f_u(\mathbf{p}_u; \mathbf{x})$. This is equivalent, however, to a determination of $p \times q_y$ parameters and is therefore equivalent to solving q_y optimization problems, where each problem is associated with p system parameters.

In order to reduce the complexity of the general problem and to ensure that each $f_u(\mathbf{p}_u; \mathbf{x})$ is evaluated using a formalism that is consistent with respect to all components, we focus on a class of problems that is characterized by a particular mathematical representation, which has its foundation in multiconvex potential theory and continuum mechanics [51]. This particular representation of systemic behavior is in fact popular within continuum mechanics and has its origins in the development of hyperelasticity. Accordingly, it is postulated that there exists a potential function $\Psi(\mathbf{p}; \mathbf{x})$ such that

$$y_u = f_u(\mathbf{p}; \mathbf{x}) = \frac{\partial \Psi(\mathbf{p}; \mathbf{x})}{\partial x_u} \tag{5}$$

This formulation effectively equips the systemic representation with a mathematical structure for determining all components y_u of the vector $\mathbf{y}$ from a single scalar potential function $\Psi(\mathbf{p}; \mathbf{x})$. An often forgotten assumption enabling this formulation is that the input and output variables can actually form a correspondence through interrelationship as conjugate pairs $\{y_u, x_u\}, u = 1, \ldots, q$, where $q = q_x = q_y$ (and therefore, this approach is not applicable for systems with mismatching cardinality of the input and output sets). In this case, the design optimization problem is reduced to that of a determination of the function $\Psi(\mathbf{p}; \mathbf{x})$. A standard technique for determining this function involves its construction as an additive linear combination of basis functions $\hat{\mathbf{a}}(\mathbf{x})$, weighted by the unknown coefficients $\mathbf{p}$ according to

$$\Psi(\mathbf{p}; \mathbf{x}) = \mathbf{p} \cdot \hat{\mathbf{a}}(\mathbf{x}) \tag{6}$$

where $\mathbf{p} = [p_1, p_2, \ldots, p_p]$ and $\boldsymbol{\beta} = [\beta_1(\mathbf{x}), \beta_2(\mathbf{x}), \ldots, \beta_n(\mathbf{x})]^T$. Another approach for construction of the function $\Psi(\mathbf{p}; \mathbf{x})$ is based on thermodynamics. This approach, which assumes that $\Psi(\mathbf{p}; \mathbf{x})$ represents an internal energy density function for many continuum systems, permits a Taylor-series expansion about the origin $\mathbf{x} = \mathbf{0}$ with respect to the state variables represented by the components forming the basis set of the input state subspace X^q. Accordingly, a second order expansion with respect to the variables x_u results in a first order constitutive theory following Eq. (5). Clearly, when terms of higher than second order are employed, the resulting systemic behavior will be nonlinear. Another important and frequently forgotten fact is that Eq. (6) is actually Eq. (2) expressed in vector notation, with the subtle difference; however, that the basis functions $\hat{\mathbf{a}}(\mathbf{x})$ are arbitrary and therefore can be selected such that their structure is more convenient for a particular system analysis. Accordingly, the structure of the basis functions $\hat{\mathbf{a}}(\mathbf{x})$ can be selected such that Eq. (6) is expressed by fewer terms relative to Eq. (2).

Substitution of Eqs. (5) and (6) into Eq. (1) yields the systemic behavior model

$$\mathbf{y} = \mathbf{p} \cdot \nabla_{\mathbf{x}} \beta(\mathbf{x}) \tag{7}$$

Within the context of continuum systems and their corresponding constitutive responses, Eqs. (1), (5)–(7) represent the behavior of the medium for all representative volume elements (RVEs) within the geometry that encloses it and is independent of shape. However, for the sake of identifying the components of the parameter vector $\mathbf{p}$, experimental measurements are to be made at discrete locations $i \in [1, \ldots, l]$ on the specimen, or in general, the system. At the same time, excitation and response are measured in terms of input-output pairs for various magnitudes of excitation indexed by $k \in [1, \ldots, m]$ for a total of m different magnitudes. Accordingly, one can construct a vector expressing the behavior of the system as calculated analytically according to

$$\mathbf{Y}_k(\mathbf{p};\mathbf{x}) = [(y_1(\mathbf{p};\mathbf{x}), \ldots, y_n(\mathbf{p};\mathbf{x}))_1, \ldots, (y_1(\mathbf{p};\mathbf{x}), \ldots, y_n(\mathbf{p};\mathbf{x}))_l]_k{}^T \tag{8}$$

and correspondingly, the behavior of the system as measured experimentally according to

$$\mathbf{Y}_k^e = [(y_1^e, \ldots, y_n^e)_1, \ldots, (y_1^e, \ldots, y_n^e)_l]_k{}^T \tag{9}$$

The quantity

$$\left\|\mathbf{Y}_k - \mathbf{Y}_k^e\right\|^2 = \sum_{j=1}^{m} (\mathbf{Y}_{kj}(\mathbf{p};\mathbf{x}) - \mathbf{Y}^e{}_{kj})^2 \tag{10}$$

expresses the square of the L_2 norm of the residual difference of $\mathbf{Y}_k$ and $\mathbf{Y}^e{}_k$ in terms of the least square difference of their respective magnitudes for each excitation increment.

The equality expressed by Eq. (10), however, must be satisfied for all excitation levels m and must be extended to include all discrete measurement positions l. This condition combined with the substitution of Eqs. (4)–(6) into Eq. (10) yields the generalized form

$$J_0 = \sum_{t=1}^{l} \sum_{j=1}^{m} (y_{jt}(\mathbf{p};\mathbf{x}) - y^e{}_{jt})^2 = \sum_{t=1}^{l} \sum_{j=1}^{m} (p_p \cdot \nabla_{\mathbf{x}} \beta(\mathbf{x}_{jt}) - y^e{}_{jt})^2 \tag{11}$$

Since this expression provides the definition of the residual error it can be used to define the objective function J_0 that when minimized yields the unknown parameter vector $\mathbf{p}$. As expected, the individual objectives folded in Eq. (11) that are related to the each individual output are satisfied as they are affected by the simultaneous presence of the rest of them.

If one assumes that linear constitutive behavior can approximate the behavior of a given system, it then follows from Eq. (4) that $\hat{\mathbf{a}}(\mathbf{x})$ must be a second order function of the components of $\mathbf{x}$. In that case, it is trivial to show that determination of Eq. (8) is reducible to a problem involving the determination of the scalar function $\Psi(\mathbf{p};\mathbf{x})$ according to

$$J_0 = (\mathbf{Bp} - \bar{\mathbf{y}}^e)^T(\mathbf{Bp} - \bar{\mathbf{y}}^e) = \sum_{s=1}^{m+l} \left(\sum_{t=1}^{n=2} B_{st} p_t - \bar{y}_s^e \right)^2 \tag{12}$$

where the overbar quantities correspond to the experimental values of the generalized work function corresponding to the inner product of the input and output vectors of the original system.

The problem expressed by Eq. (12) can be solved by methods based on the solution of normal equations (normal-equations method), QR factorization, or singular value decomposition (SVD) [50]. Selecting one of these methods to determine the unknown model parameters can be a process that depends on ranking these methods with regard to their performance in terms of attributes or metrics that are important to the user. It has been documented, for example, that the normal equation method is computationally fast and requires less resources, but is less accurate. In contrast, it is well known that SVD requires substantial computational resources, but is more reliable and accurate than other methods.

In all material characterization cases that follow, the material parameters will be determined in a manner that follows this section as a general template, in the sense of solving optimization problems that minimize objective functions constructed as described in this section.

The Case of One-Dimensional Material System

To introduce design optimization for material characterization in a fashion of increasing complexity, we consider first a one-dimensional system that possesses both linear recoverable and nonlinear irrecoverable responses. The template approach that we will employ first for this simple case and then for more realistic cases is that of defining a strain energy density (SED) function that governs the material behavior and indirectly contains the actual constitutive behavior.

$$U_{1D} = U_{1D}^R(S,\varepsilon) + U_{1D}^I(S,\beta_i;\varepsilon) = \left[\frac{1}{2} S\varepsilon^2\right]_{1D}^R + \left[D(\beta_i;\varepsilon)\frac{1}{2} S\varepsilon^2\right]_{1D}^I \tag{13}$$

where $U_{1D}^R(S,\varepsilon)$ and $U_{1D}^I(S,\beta_i;\varepsilon)$ are the recoverable (elastic) SED and the irrecoverable (inelastic or dissipated) SED, respectively. The quantities S, β_i, and $D(S,\beta_i;\varepsilon)$ are the stiffness constant (modulus of elasticity), the constants participating in the dissipated energy coefficient function, and the dissipated energy density coefficient function, itself, respectively. Equation (13) implies that the irrecoverable or dissipated strain energy density (DSED) has been constructed to be a multiplicative decomposition with weighting $D(\beta_i;\varepsilon)$ for the recoverable SED according to:

$$U_{1D}^I(C,\beta_i;\varepsilon) = D(\beta_i;\varepsilon) U_{1D}^R(S,\varepsilon) \tag{14}$$

The functional form of $D(\beta_i;\varepsilon)$ should be one that ensures energy dissipation in a manner that yields a softening of nonlinear stress-strain constitutive response. There are many forms that have this property, based on transcendental functions, which have been used in the past [47]. Here, we employ a functional form that can be expanded in a Taylor-series. This functional form provides for a polynomial representation that is a necessary condition for algebraic reducibility and is therefore convenient for algebraic transformations. This form of the DSED, which is initially negligible and then monotonically increasing, can be represented by the following physically consistent choice of $D(\beta_i;\varepsilon)$

$$D(\beta_i;\varepsilon) = D(m,\varepsilon_f;\varepsilon) = 1 - e^{-(1/me)\left(\varepsilon/\varepsilon_f\right)^m} \tag{15}$$

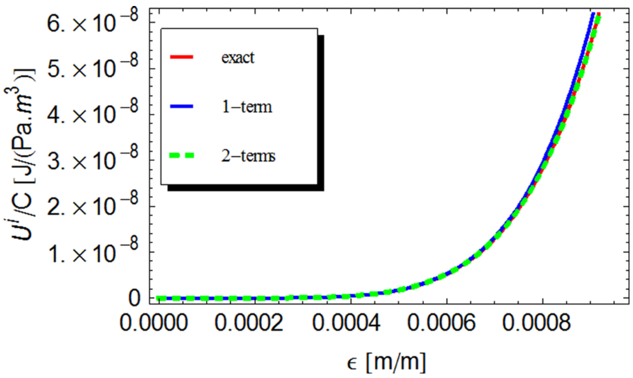

Fig. 3 Difference of 1- and 2-term approximations of normalized irrecoverable or dissipated energy density as a function of strain relative to the exact model

where $\beta_1 = m$ and $\beta_2 = \varepsilon_f$ are the two material parameters controlling the dissipative nature of the material behavior. The exponent m controls the level of nonlinearity involved in the model, and ε_f expresses the level of failure strain. The series expansion of $\bar{D}(m, \varepsilon_f; \varepsilon)$ defined by Eq. (15) yields

$$\bar{D}(m, \varepsilon_f; \varepsilon) = \sum_{k=1}^{n} \frac{(-1)^k}{k!} \left(\frac{1}{me}\right)^k \left(\frac{\varepsilon}{\varepsilon_f}\right)^{mk} \tag{16}$$

Given Eqs. (16) and (13), it follows that Eq. (14) may be expressed by

$$U_{1D}^{I}(S, \beta_i; \varepsilon) = \frac{1}{2} S \sum_{k=1}^{n} \frac{(-1)^k}{k!} \left(\frac{1}{me}\right)^k \left(\frac{\varepsilon}{\varepsilon_f}\right)^{mk} \varepsilon^2 \tag{17}$$

A plot of the function defined by Eq. (17), normalized by the Elastic constant S, is presented in Fig. 3 for $m = 4$ and $\varepsilon_f = 0.0008$. Referring to Fig. 3, it can be seen that for more than two terms the series expression gives essentially identical results to those of the exact evaluation of DSED. It is interesting to note that the single term expression is also in good agreement with the exact form. Therefore, we can truncate all but the first term in Eq. (17) to obtain

$$U_{1D}^{I}(S, \beta_i; \varepsilon) = -\frac{1}{2} S \left(\frac{1}{me}\right) \left(\frac{\varepsilon}{\varepsilon_f}\right)^{m} \varepsilon^2 \tag{18}$$

It follows then that Eq. (13) can be expressed

$$U_{1D} = U_{1D}^{R}(S, \varepsilon) + U_{1D}^{I}(S, \beta_i; \varepsilon) = \frac{1}{2} S\varepsilon^2 - \frac{1}{2} S \left(\frac{1}{me}\right) \left(\frac{\varepsilon}{\varepsilon_f}\right)^{m} \varepsilon^2 \tag{19}$$

According to Eq. (7), the corresponding constitutive law will be given by

$$\begin{aligned} \sigma_{1D} &= \frac{\partial [U_{1D}^{R}(S, \varepsilon) + U_{1D}^{I}(S, \beta_i; \varepsilon)]}{\partial \varepsilon} \\ &= \sigma_{1D}^{R}(S, \varepsilon) + \sigma_{1D}^{I}(S, \beta_i; \varepsilon) \\ &= S\varepsilon - S \left(\frac{2 + m}{2me}\right) \left(\frac{\varepsilon^{m+1}}{\varepsilon_f{}^{m}}\right) \end{aligned} \tag{20}$$

The resulting constitutive law contains the linear elastic part, as expected, that is modified by a nonlinear inelastic term. An indicative variation of total SED and its components (recoverable and irrecoverable SEDs), as described by Eq. (19), are shown in Fig. 4(*a*). Figure 4(*b*) shows the corresponding stress distribution defined by the constitutive law expressed by Eq. (20).

In the present formulation, the material parameters to be identified, or estimated based on experimental data, are the stiffness parameter, S, and the two dissipated energy parameters m and ε_f.

The results of applying design optimization for determining these material parameters for 20 data points created synthetically by using the material model defined Eq. (19) or (20) are shown in Table 1 for three global optimization methods implemented by the "NMinimize" function call in MATHEMATICA 7.0 [51]. The minimization was performed on the objective function defined by Eq. (10), where $\mathbf{Y}_k = \{U_{1d,k}\}^T$ and $\mathbf{Y}_k^e = \{U_{1d,k}^e\}^T$, and therefore the problem is a nonlinear optimization one. The methods utilized were the Nelder Mead (also called downhill simplex method or amoeba method nonlinear optimization technique, which is a well-defined numerical method for twice differentiable and unimodal problems), the differential evolution (which optimizes a problem by iteratively trying to improve a candidate solution with regard to a given measure of quality) and the Simulated Annealing methods.

The criterion used by MATHEMATICA to exit from the optimization loop is to make the numerical error in the result of size x be less than $10^{-8}(1 + |x|)$ or reach 550 iterations except for the case of simulated annealing that required a maximum iteration limit of 5000.

These results indicate that Nelder-Mead and differential evolution methods are able to determine the properties exactly, while simulated annealing takes much longer and achieves less accurate parameter determinations.

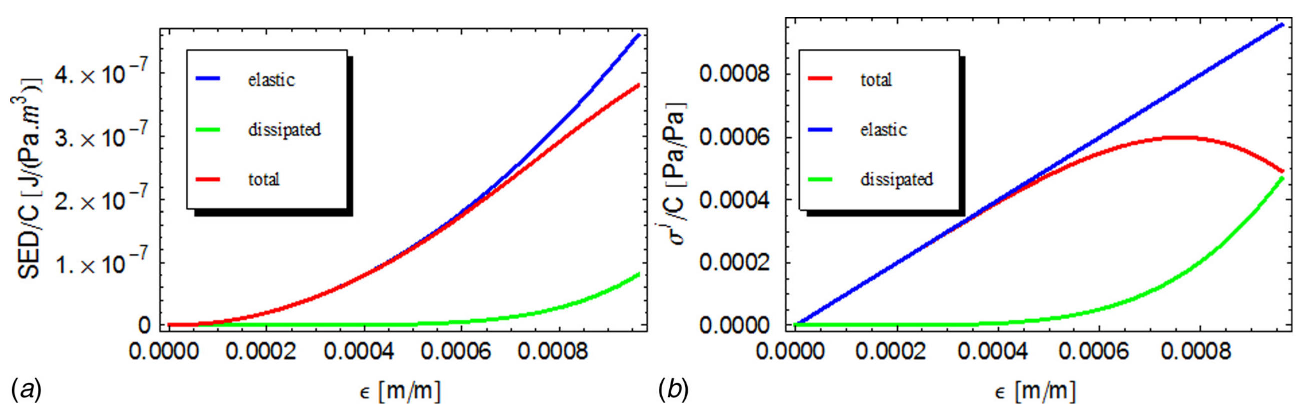

Fig. 4 Distribution of elastic, dissipated (or irrecoverable) and total SEDs for one-dimensional case (*a*) and corresponding stress distributions as a function of strain (*b*)

Table 1 Design optimization results for a nonlinear 1D material system

Method	Objective function	C(GPa)	m	ε_f
Target values	0.00	130.00	4	0.0008
Nelder Mead	−0.0000116825	130.00	4	0.0008
Differential evolution	$-4.29153 * 10^{-6}$	130.00	4	0.0008
Simulated annealing	134,234	131.21	3.1	0.000856

Composite Material System

For the general case of a composite material system, we consider that a modified anisotropic hyperelastic strain energy density function can be constructed to encapsulate both the elastic and the inelastic responses of the material. However, certain classes of composite materials reach failure after small strains and some under large strains. For this reason, we give two examples, one involving a small (infinitesimal) strain formulation (SSF) and another involving a finite (large) strain formulation (FSF).

Small Strain Formulation. For the SSF, we introduce a SED function that, in its most general form, can be represented as a scaled Taylor expansion of the Helmholtz free energy of a deformable body, which is in terms of small strain invariants of the form

$$\begin{aligned} U_{\mathrm{SSF}}(I_1,I_2,I_3) &= s_0 + s_{11}I_1 + \frac{1}{2}s_{12}I_1^2 + \frac{1}{3!}s_{13}I_1^3 + \frac{1}{4!}s_{14}I_1^4 \\ &+ \cdots + s_{21}I_2 + \frac{1}{2}s_{22}I_2^2 + \frac{1}{3!}s_{23}I_2^3 + \frac{1}{4!}s_{24}I_2^4 \\ &+ \cdots + \frac{1}{2}s_{13}I_3^2 + \frac{1}{3!}s_{13}I_3^3 + \frac{1}{4!}s_{14}I_3^4 + \cdots \\ &+ \frac{1}{2}s_{1121}I_1I_2 + \frac{1}{3!}s_{1221}I_1^2I_2 + \frac{1}{3!}s_{1122}I_1I_2^2 + \cdots \\ &+ \frac{1}{2}s_{1131}I_1I_3 + \frac{1}{3!}s_{1331}I_1^2I_3 + \frac{1}{3!}s_{1133}I_1I_3^2 + \cdots \\ &+ \frac{1}{4!}s_{1321}I_1^3I_2 + \frac{1}{4!}s_{1221}I_1^2I_2^2 + \frac{1}{4!}s_{1123}I_1I_2^3 + \cdots \end{aligned} \tag{21}$$

where the invariants are defined by

$$I_1 = \mathrm{tr}(\boldsymbol{\varepsilon}) = \varepsilon_{ii}, \quad I_2 = \frac{1}{2}\mathrm{tr}(\boldsymbol{\varepsilon}^2) = \frac{1}{2}\varepsilon_{ij}\varepsilon_{ij}, \quad I_3 = \frac{1}{2}\mathrm{tr}(\boldsymbol{\varepsilon}^3) = \frac{1}{3}\varepsilon_{ij}\varepsilon_{jk}\varepsilon_{ki} \tag{22}$$

The invariants are chosen to guarantee the a priori knowledge that the SED as a scalar quantity must be invariant under frame reference translations and rotations. This follows in that the SED should be objective (i.e., independent of the observer's frame of reference).

An additive decomposition of this expression in terms of a recoverable and an irrecoverable SED can be expressed by

$$U_{\mathrm{SSF}} = U^R_{\mathrm{SSF}}(\mathbf{S};\varepsilon_{ij}) + U^I_{\mathrm{SSF}}(\mathbf{D};\varepsilon_{ij}) \tag{23}$$

Clearly, all the second order monomials of strain components will be forming the recoverable part $U^R_{\mathrm{SSF}}(\mathbf{S};\varepsilon_{ij})$ and the higher order monomials will be responsible for the irrecoverable part $U^I_{\mathrm{SSF}}(\mathbf{D};\varepsilon_{ij})$. The resulting constitutive law is be given by

$$\begin{aligned} \sigma_{ij} &= \partial U_{\mathrm{SSF}}/\partial\varepsilon_{ij} \\ &= \partial(U^R_{\mathrm{SSF}}(\mathbf{S};\varepsilon_{ij}) + U^I_{\mathrm{SSF}}(\mathbf{D};\varepsilon_{ij}))/\partial\varepsilon_{ij} \\ &= \frac{\partial U_{\mathrm{SSF}}}{\partial I_1}\frac{\partial I_1}{\partial\varepsilon_{ij}} + \frac{\partial U_{\mathrm{SSF}}}{\partial I_2}\frac{\partial I_2}{\partial\varepsilon_{ij}} + \frac{\partial U_{\mathrm{SSF}}}{\partial I_3}\frac{\partial I_3}{\partial\varepsilon_{ij}} \end{aligned} \tag{24}$$

A general expression which provides a strain-dependent version of Eq. (23), is given by

$$U_{\mathrm{SSF}} = U^R_{\mathrm{SSF}}(\mathbf{S};\varepsilon_{ij}) + U^I_{\mathrm{SSF}}(\mathbf{D};\varepsilon_{ij}) = \frac{1}{2}s_{ijkl}\varepsilon_{ij}\varepsilon_{kl} + d_{ijkl}(\varepsilon_{ij})\varepsilon_{ij}\varepsilon_{kl} \tag{25}$$

where s_{ijkl} are the components of the elastic stiffness tensor (Hooke's tensor) and $d_{ijkl}(\varepsilon_{ij})$ are strain-dependent damage functions, which fully define irrecoverable or dissipated strain energy density given by enforcing the dissipative nature of energy density. The quantity $d_{ijkl}(\varepsilon_{ij})$ is given by

$$d_{ijkl}(\varepsilon_{ij}) = s_{ijkl}\left(1 - e^{(-(\varepsilon_{ij}/q_{ij}))^{p_{ij}}/(ep_{ij})}\right) \tag{26}$$

This is done in a manner analogous to that employed for the 1D system described above. As in the 1D case, we perform an equivalent series expansion and subsequently drop all terms except the first, in that it captures almost all of the dissipative behavior. Accordingly,

$$\begin{aligned} d_{ijkl}(\varepsilon_{ij}) &= s_{ijkl}\sum_{m=1}^{n}(-1)^m\left(\frac{1}{ep_{ij}}\right)^m \frac{\varepsilon_{ij}{}^{mp_{ij}}}{m!q_{ij}{}^{mp_{ij}}} \\ &= s_{ijkl}\left(-\left(\frac{1}{ep_{ij}}\right)\frac{\varepsilon_{ij}{}^{p_{ij}}}{q_{ij}{}^{p_{ij}}} + \left(\frac{1}{ep_{ij}}\right)^2\frac{\varepsilon_{ij}{}^{2p_{ij}}}{2q_{ij}{}^{2p_{ij}}} - \cdots + \right) \\ &\simeq -s_{ijkl}\left(\frac{1}{ep_{ij}}\right)\frac{\varepsilon_{ij}{}^{p_{ij}}}{q_{ij}{}^{p_{ij}}} \end{aligned} \tag{27}$$

Thus, the irrecoverable part of the energy in Eq. (23) becomes

$$\begin{aligned} U^I_{\mathrm{SSF}}(\mathbf{D};\varepsilon_{ij}) &= U^I_{\mathrm{SSF}}(s_{ijkl},p_{ij},q_{ij};\varepsilon_{ij}) \\ &= -s_{ijkl}\frac{1}{e(2+p_{ij})p_{ij}q_{ij}{}^{p_{ij}}}\varepsilon_{ij}{}^{1+p_{ij}}\varepsilon_{kl} \end{aligned} \tag{28}$$

Next, substituting Eq. (26) into Eq. (23) yields

$$\begin{aligned} U_{\mathrm{SSF}} &= U^R_{\mathrm{SSF}}(\mathbf{S};\varepsilon_{ij}) + U^I_{\mathrm{SSF}}(\mathbf{D};\varepsilon_{ij}) \\ &= \frac{1}{2}s_{ijkl}\varepsilon_{ij}\varepsilon_{kl} - s_{ijkl}\frac{1}{e(2+p_{ij})p_{ij}q_{ij}{}^{p_{ij}}}\varepsilon_{ij}{}^{1+p_{ij}}\varepsilon_{kl} \end{aligned} \tag{29}$$

Applying Eq. (22) on Eq. (27), and employing matrix [3] notation for the case of a general orthotropic material, yields the constitutive relation

$$\begin{bmatrix}\sigma_{xx}\\ \sigma_{yy}\\ \sigma_{zz}\\ \sigma_{xz}\\ \sigma_{yz}\\ \sigma_{xy}\end{bmatrix} = \begin{bmatrix} s_{xx}(1-\bar{d}_{xx}) & s_{xy} & s_{xz} & & & \\ s_{xy} & s_{yy}(1-\bar{d}_{yy}) & s_{yz} & & & \\ s_{xz} & s_{yz} & s_{zz}(1-\bar{d}_{zz}) & & & \\ & & & s_{xz}(1-\bar{d}_{xz}) & & \\ & & & & s_{yz}(1-\bar{d}_{yz}) & \\ & & & & & s_{zz}(1-\bar{d}_{xy}) \end{bmatrix} \begin{bmatrix}\varepsilon_{xx}\\ \varepsilon_{yy}\\ \varepsilon_{zz}\\ \gamma_{xz}\\ \gamma_{yz}\\ \gamma_{xy}\end{bmatrix} \tag{30}$$

where

$$\bar{d}_{ij} = \frac{1}{ep_{ij}q_{ij}^{p_{ij}}}\varepsilon_{ij}{}^{1+p_{ij}} \tag{31}$$

All terms that are not shown in expression (30) are zero due to the orthotropic symmetry requirements. Therefore, the material parameters are the nine elastic constants s_{ij} and the $6 \times 2 = 12$ damage constants p_{ij}, q_{ij} for a total of 21 parameters. Clearly, when the quantities $\bar{d}_{ij}$ do not depend on the strains and they are constant, Eq. (28) reduces to most of the continuous damage theories given by various investigators in the past [46,52–55]. For a transversely isotropic material, the number of material parameters drops to $5+10=15$ for a 3D state of strain and to $4+8=12$ for a plane stress state.

Finite Strain Formulation. The FSF can be written in a double additive decomposition manner. The first being the decomposition of the recoverable and irrecoverable SED, and the second being the decomposition between the volumetric (or dilatational) W_v and the distortional (or isochoric) W_d parts of the total SED. For a material with two principal directions, this decomposition can be expressed by [56]

$$\begin{aligned} U_{\mathrm{SSF}} &= U^R_{\mathrm{SSF}}(\alpha_i; J, \bar{\boldsymbol{C}}) + U^I_{\mathrm{SSF}}(\alpha_i, \beta_i; J, \bar{\boldsymbol{C}}) \\ &= [W_v(J) + W_d(\bar{\boldsymbol{C}}, \mathbf{A}\otimes\mathbf{A}, \mathbf{B}\otimes\mathbf{B})] \\ &\quad - [d_v W_v(J) + d_d W_d(\bar{\boldsymbol{C}}, \mathbf{A}\otimes\mathbf{A}, \mathbf{B}\otimes\mathbf{B})] \end{aligned} \tag{32}$$

where α_i, β_i are the elastic and inelastic material parameters of the system, respectively. A rearrangement of these decompositions, such as the volumetric versus distortional decomposition, which appears on the highest expression level, leads to an expression introduced in Ref. [56], i.e.,

$$U_{\mathrm{FSF}} = (1-d_v)W_v(J) + (1-d_d)W_d(\bar{\boldsymbol{C}}, \mathbf{A}\otimes\mathbf{A}, \mathbf{B}\otimes\mathbf{B}) \tag{33}$$

with the damage parameters $d_k \in [0,1], k \in [v,d]$ defined as

$$d_k = d^{\infty}_{ka}\left[1 - e^{(-(a_k(t)/\eta_{ka}))}\right] \tag{34}$$

where $a_k(t) = \max_{s\in[0,t]} W^o_k(s)$ is the maximum energy component reached so far, and d^{∞}_{ka} and η_{ka} are the two pairs of parameters controlling the energy dissipation characteristics of the two components of SED. In this formulation, $J = \det \underline{\mathbf{F}}$ is the deformation gradient, $\bar{\boldsymbol{C}} = \underline{\mathbf{F}}^T.\underline{\mathbf{F}}$ is the right Cauchy Green (Green deformation) tensor, $\mathbf{A}$ and $\mathbf{B}$ are the constitutive material directions in the undeformed configuration, and $\mathbf{A}\otimes\mathbf{A}$ and $\mathbf{B}\otimes\mathbf{B}$ are microstructure structural tensors expressing fiber directions. Each of the two components of SED are defined as

$$\begin{aligned} W_v(J) &= \frac{1}{d}(J-1)^2 \\ W_d(\bar{\boldsymbol{C}}, \mathbf{A}\otimes\mathbf{A}, \mathbf{B}\otimes\mathbf{B}) &= \sum_{i=1}^{3} a_i(\bar{I}_1-3)^i + \sum_{j=1}^{3} b_j(\bar{I}_2-3)^j \\ &\quad + \sum_{k=1}^{6} c_k(\bar{I}_4-1)^k + \sum_{l=2}^{6} d_l(\bar{I}_5-1)^l \\ &\quad + \sum_{m=2}^{6} e_m(\bar{I}_6-1)^m + \sum_{n=2}^{6} f_n(\bar{I}_7-1)^n \\ &\quad + \sum_{o=2}^{6} g_o(\bar{I}_8-(\mathbf{A}\cdot\mathbf{B})^2)^o \end{aligned} \tag{35}$$

where the strain invariants are defined as follows:

$$\begin{aligned} &\bar{I}_1 = tr\bar{\boldsymbol{C}}, \quad \bar{I}_2 = \frac{1}{2}(tr^2\bar{\boldsymbol{C}} - tr\bar{\boldsymbol{C}}^2) \\ &\bar{I}_4 = \mathbf{A}\cdot\mathbf{C}\mathbf{B}, \quad \bar{I}_5 = \mathbf{A}\cdot\bar{\boldsymbol{C}}^2\mathbf{B} \\ &\bar{I}_6 = \mathbf{B}\cdot\mathbf{C}\mathbf{B}, \quad \bar{I}_7 = \mathbf{B}\cdot\bar{\boldsymbol{C}}^2\mathbf{B}, \quad \bar{I}_8 = (\mathbf{A}\cdot\mathbf{B})\mathbf{A}\cdot\bar{\boldsymbol{C}}B \end{aligned} \tag{36}$$

The corresponding constitutive behavior is given by the second Piola-Kirchhoff stress tensor according to [52]

$$S = 2\frac{\partial U_{\mathrm{FSF}}}{\partial C} \tag{37}$$

or the usual Cauchy stress tensor according to

$$\sigma_{\mathrm{FSF}} = \frac{2}{J}\mathbf{F}\cdot\frac{\partial U_{\mathrm{FSF}}}{\partial C}\cdot\mathbf{F}^T \tag{38}$$

Note that both of the last two relations follow the general form described in Eq. (5). Under the FSF formulation, the material characterization problem involves determining the 36 coefficients (at most) of all monomials when the sums in the expression of distortional SED are expanded in Eq. (15), in addition to the compressibility constant d and the four parameters used in Eq. (14). It follows that potentially there can be a total of 41 material constants.

Numerical Results

For the purpose of demonstrating numerically the aforementioned concepts, the material selected for generating the necessary simulated experimental data is a typical laminate constructed from an epoxy resin/fiber laminae system of type AS4/3506-1. The elastic moduli of this material are listed in Table 2 according to several sources [3,54,57–62].

Clearly, what is considered to be a set of material constants varies widely as it really depends on the fiber volume fraction, the

Table 2 Engineering properties of AS4/3506-1 laminae

Ref	E_{11} (GPa)	E_{22} (GPa)	E_{22} (GPa)	v_{12}	v_{23}	v_{13}	G_{12} (GPa)	G_{23} (GPa)	G_{13} (GPa)
[3]	147.0	10.3	10.3	0.27	0.28	0.27	7.0	4.04	7.0
[54]	142.0	9.8	9.8	0.30	0.34	0.30	6.0	3.77	6.0
[57]	135.0	9.0	9.0	0.28		0.28	6.9		6.9
[58]	138.0	9.7	9.7	0.30	0.49	0.30	5.24	3.24	5.24
[59]	139.3	11.1	11.1	0.30	0.40	0.30	6.0	3.964	6.0
[60]	150.0	8.0	8.0	0.30		0.30	5.0		5.0
[61]	147.0	10.3	10.3	0.27		0.27	6.89		6.89
[62]	142.0	10.3	10.3	0.27		0.27	7.2		7.2
Min	135.0	8.0	8.0	0.27	0.28	0.27	5.0	3.24	5.0
Avg.	142.5	9.8	9.8	0.29	0.30	0.29	6.279	3.753	6.279
Max.	150.0	11.1	11.1	0.30	0.49	0.30	7.2	4.039	7.2
Deviation (%)	11.1	38.8	38.8	11.1	78.2	11.1	44.0	24.7	44.0
Avg. cons.	142.5	9.81	9.81	0.29	0.30	0.29	6.279	3.769	6.279

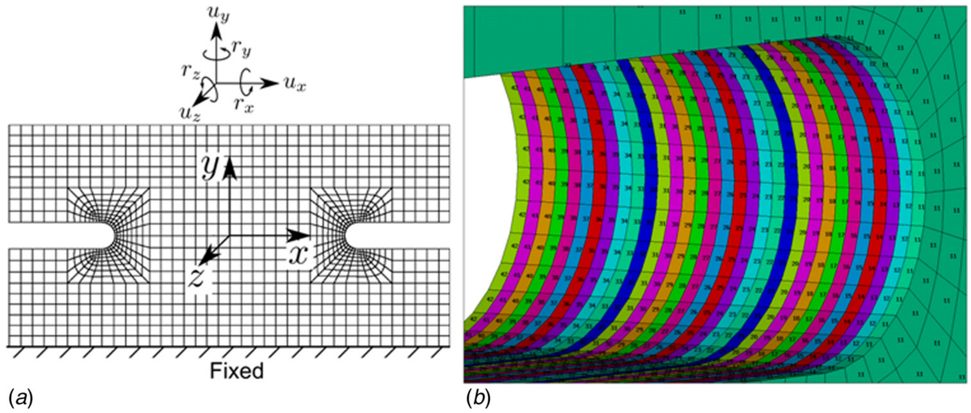

Fig. 5 Discretization and boundary conditions of typical specimen used for material characterization (*a*) and detail of FEA model near one of the notches (*b*)

fiber coating, and the manufacturing process of the fiber, resin, and composite. As can be seen from the bottom of the entries of the table where we added some statistical observations, % deviation observed varies from 11.1% to 78.2%. It is therefore important to identify the set of elastic material properties before and after a batch of new material is manufactured or before a material system is used for design, material qualification, or material certification. To demonstrate the usage of the SSF in conjunction with design optimization, we present here an example of using real data form a multiaxially loaded specimen from a test conducted by utilizing NRL66.3. The model characteristics of the specimen used are presented in Fig. 5, where on the left, the discretization model and potential boundary conditions are depicted, and on the right, a detail at the area of the left notch shows a stacking of $[+60, -60]_{16}$ with each lamina made out of AS4/3506-1.

Two objective functions were constructed. Both utilized the fact that through the REMDIS-3D software, developed by our group, one can obtain full field measurements of the displacement and strain fields over any deformable body [24–28]. The mesh-free representation of the displacement and strain fields throughout the entire field of view allows the calculation of the experimentally measured values at any point on the specimen surface, including the nodal points of the FEM analysis utilized for the forward computation of the direct problem embedded in the optimization loop. Our software has the capability of accepting the nodal coordinate specification generated by the FEA as a definition for exporting the required quantities at these points. Thus, our experimental measurements for the formation of the objective functions were chosen to be the strains at the nodal points of the discretization shown Fig. 5. The first objective function chosen was based entirely on strains and is given by

$$J^{\varepsilon} = \sum_{k=1}^{N} \left(\sum_{i=1}^{2} \sum_{j=i}^{2} \left(\left[\varepsilon_{ij}^{\text{exp}}\right]_k - \left[\varepsilon_{ij}^{\text{fem}}\right]_k \right) \right)^2 \tag{39}$$

and the second objective function is given in terms of surface strain energy density according to

$$J^U \approx \oint_{\partial\Omega} \left(U^{\text{exp}} - U^{\text{fem}}\right)^2 dS$$
$$\approx \left[\oint_{\partial\Omega} \left(\sum_{i=1}^{2} \sum_{j=i}^{2} \sum_{m=1}^{2} \sum_{n=m}^{2} \left(s_{ijmn}\varepsilon_{ij}^{\text{exp}}\varepsilon_{mn}^{\text{exp}} - s_{ijmn}\varepsilon_{ij}^{\text{fem}}\varepsilon_{mn}^{\text{fem}} \right) \right)^2 dS \right] \tag{40}$$

where $[\varepsilon_{ij}^{\text{exp}}]_k$ and $[\varepsilon_{ij}^{\text{fem}}]_k$ are the experimentally determined and the FEM produced components of strain are at node k. The quantities U^{exp} and U^{fem} are the values of the surface strain energy density formulated by using the experimental strains and the FEM produced strains, respectively.

It is worthwhile to mention here that, because it is not experimentally possible to obtain through-thickness strain data, with any full field strain measurement method, we formulated the objective functions only in terms of the surface strains as is evident by the fact that the indices in Eqs. (38) and (39) do not take the value 3 to account for the through-thickness components of strain.

The formal optimization problem for all objective functions in the present work, can be stated as follows:

$$\min J(s_{ijnm}) \tag{41a}$$

$$\text{subject to } g_k(s_{ijnm}) \leq 0, k = 1, 2, \ldots, K \tag{41b}$$

$$h_l(s_{ijnm}) = 0, l = 1, 2, \ldots, L \tag{41c}$$

$$s_{ijnm}^L \leq s_{ijnm} \leq s_{ijnm}^U, i, j, n, m = 1, 2, 3 \tag{41d}$$

where the design variables s_{ijnm} should be considered as the material parameters to be determined and where Eqs. (41*b*) and (41*c*) express potentially active inequality and equality constraints, respectively, and Eq. (41*d*) expresses the design space bounding constrains.

For our case throughout the present paper, there are no physically or mathematically justified constrains. However, since we know the class of materials we are involved with, we can select bounding domains that are justified on the basis of their positive definiteness (for all SSF parameters) and reasonable selections for low and upper bounds selected strictly to reduce the numerical search time of the used optimizers.

An implementation of this optimization for both objective functions was applied by using the DIRECT global optimizer [63], which is available for MATLAB [64], and a custom developed Monte-Carlo optimizer as described in Ref. [65], also implemented in MATLAB. The DIRECT global optimizer was significantly slower than the Monte Carlo and therefore here we are reporting the results of the Monte Carlo optimizer. Since the results from implementing both objective functions were virtually identical here we are reporting only those corresponding to Eq. (38). The convergence criterion for exiting the optimization loop was $J^U < 2\text{e} - 6$ and the optimization was completed after 1562 evaluations in about 11 h. The calculation of the objective function integral was done on 2493 nodes and the forward part of the calculation was implemented on ANSYS Mechanical [66].

The loading conditions applied for the moveable edge of the specimen were $u_x = 0$ [m], $u_y = 0.0005$ [m], $u_z = 0.001$ [m], $r_x = 0$ [rad], $r_y = 0$ [rad], $r_z = 0$ [rad]. The bounds of the design variables (engineering constants) were $E_{11}, E_{22} \in [1e9, 5e11]$ Pa,

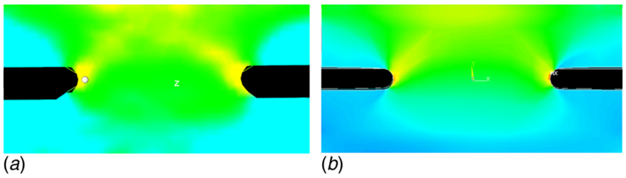

Fig. 6 Distributions of the vertical component of strain (ε_{yy}) as determined experimentally via MRGM (*a*) and the corresponding matched distribution of the numerical model as it was produced by FEA (*b*) for the purpose of determining the five elastic constants of AS4/3506-1 composite lamina material

$\nu_{12}, \nu_{23} \in [0.1, 0.9]$, and $G_{12} \in [5e8, 5e10]$ Pa. A preliminary sensitivity analysis on the potential bounds suggested that neither the optimization performance nor accuracy are greatly affected by this choice, as long as their values are sensible.

In Fig. 6, we can see the experimentally acquired distribution of ε_{yy} (left) and the corresponding distribution produced from FEM analysis for the five identified unique elastic constants, which are shown in Table 3, in comparison to those of Ref. [3].

For the case of the FSF, a two stage optimization was performed. In the first stage, we determined the values of the coefficients of the strain invariant monomials in Eq. (35) such that the FSF matches the SSF by constructing and minimizing an objective function of the form

$$J^{\mathrm{URF}}(d, a_1, b_1, c_1, d_1) \approx \oint_{\partial\Omega} (U^R_{\mathrm{FSF}} - U^R_{\mathrm{SSF}})^2 dS \approx \left[\oint_{\partial\Omega} \left(\sum_{i=1}^{2} \sum_{j=i}^{2} \sum_{m=1}^{2} \sum_{n=m}^{2} (U^R_{\mathrm{FSF}} - U^R_{\mathrm{SSF}}) \right)^2 dS \right] \tag{42}$$

This was done is order to establish the proper parameters of the FSF model that match the SSF model.

In the second stage, the material parameters encoding the damage behavior of the FSF were determined through the minimization of the objective function

$$\begin{aligned} J^{\mathrm{UF}}&(d, a_1, b_1, c_1, d_1, d_a^{\infty}, \eta_a) \\ &\approx \oint_{\partial\Omega} (U^1_{\mathrm{FSF}} - U^2_{\mathrm{FSF}})^2 dS \\ &\approx \left[\oint_{\partial\Omega} \left(\sum_{i=1}^{2} \sum_{j=i}^{2} \sum_{m=1}^{2} \sum_{n=m}^{2} (U^1_{\mathrm{FSF}} - U^2_{\mathrm{FSF}}) \right)^2 dS \right] \end{aligned} \tag{43}$$

where $U^1_{\mathrm{FSF}}(\bar{d}, \bar{a}_1, \bar{b}_1, \bar{c}_1, \bar{d}_1, \bar{d}_a^{\infty}, \bar{\eta}_a)$ is the SED of the FSF for the parameters $\bar{d}, \bar{a}_1, \bar{b}_1, \bar{c}_1, \bar{d}_1$ computed from the previous step of matching the FSF with the SSF. The parameters $\bar{d}_a^{\infty}$ and $\bar{\eta}_a$ were chosen arbitrarily to be some values that can capture nonlinearity due to damage. This complete set of parameters represents the known target model of the material as shown in the second row of Table 4. The unknown constitutive model was chosen to be represented by another FSF SED, namely $U^1_{\mathrm{FSF}}(d, a_1, b_1, c_1, d_1, d_a^{\infty}, \eta_a)$. The bottom row of Table 4 shows the parameters determined by minimizing the objective function in Eq. (43) via a Monte-Carlo global optimizer.

Table 3 Engineering properties of AS4/3506-1 laminae

Ref	E_{11} (GPa)	E_{22} (GPa)	ν_{12}	ν_{23}	G_{12} (GPa)
Daniels [3]	147.0	10.3	0.27	0.28	7.0
Present	125.0	10.8	0.27	0.32	7.96

Table 4 FSF parameters of AS4/3506-1 laminae with damage

Model	d	a_1	b_1	c_1	e_1	d_a^{∞}	η_a
Target	0.00007012	1611	713	29212	-458.7	0.9	1.8
Identified	0.00006987	1613	721	29105	-449.3	0.92	1.979

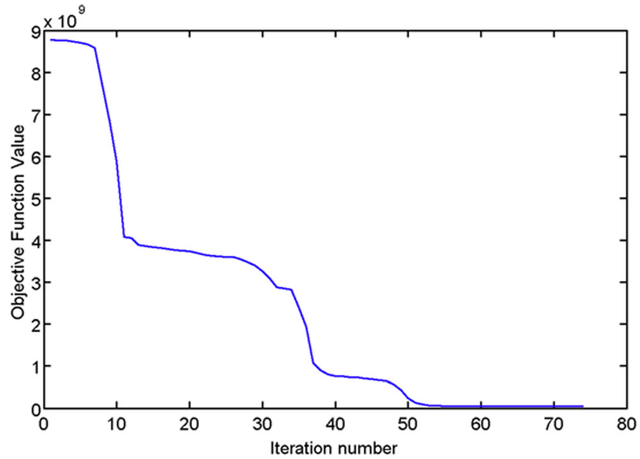

Fig. 7 Decay of the objective function versus iteration number

The convergence criterion for exiting the optimization loop was $J^{\mathrm{UF}} < 2\mathrm{e}4$ and the optimization was completed after 2748 evaluations in about 29 h. The calculation of the objective function integral was done also on 2493 nodes.

The bounds of the design variables (engineering constants) were $d \in [1e-6, 1e-7]$, $a_1, b_1 \in [1e2, 1e4]$, $c_1 \in [1e2, 1e4]$, $e_1 \in [-1e4, 1e4]$, $d_a^{\infty} \in [0.3, 1.0]$, and $\eta_a \in [1.0, 2.0]$.

It should be noted that since energy-conforming limits have not been established for the parameters of the FSF model, a penalty factor was introduced in the optimizer for the cases the energetic formulation in the FEA was nonconforming.

For this case, the evolution of the objective function versus iteration steps is shown in Fig. 7.

An indication of how well the FSF can capture the SSF, for the case of the recoverable (linear elastic) regime, is shown in Fig. 8, where the distribution of ε_{yy} is shown for both models for a case of combined torsion and tension of the specimen. In addition, a comparison of load versus strain evolution, for a point in front of the first of two notches, is shown in Fig. 9.

Conclusions and Discussion

In an effort to provide an overview of mechatronically and computationally automated research, we have demonstrated the application of design optimization methodologies for the determination of the constitutive response of composite materials with or without damage. Strain energy density and a custom developed mesh-free full field strain measurement based approaches have been utilized to incorporate massive full field strain measurements from specimens loaded by a multiaxial custom-made loading machine. We have formulated objective functions expressing the difference between the experimentally observed behavior of composite materials under various loading conditions, and the simulated behavior via FEA, which are formulated in terms of strain energy density functions of a particular structure under identical loading conditions.

Two formalisms involving small strains and finite strains have been utilized in a manner that involves both additive decomposition of recoverable and irrecoverable strain energy densities. This was done in order to address both the elastic and inelastic

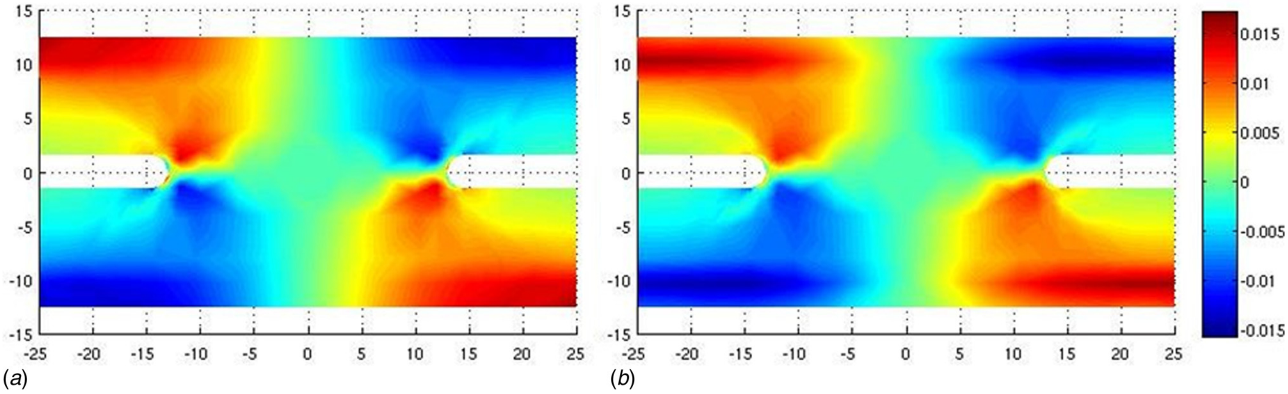

Fig. 8 Comparison between the small strain formulation FEA results of the vertical component of strain (ε_{yy}) (*a*) and the corresponding finite formulation results (*b*) for the case of a specimen loaded both in tension and torsion

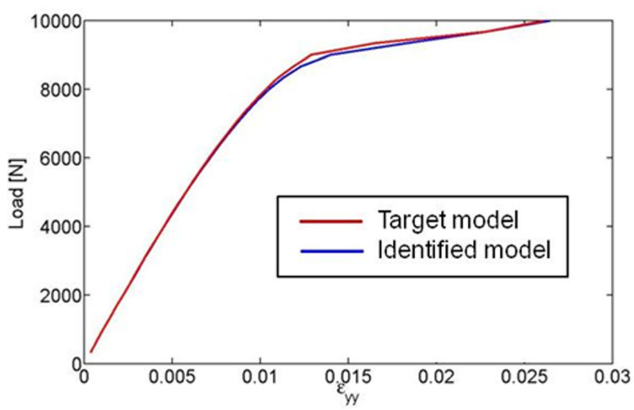

Fig. 9 Comparison of the load versus the vertical component of strain (ε_{yy}) at a point in front of the notch, between the target and the identified model by using the FSF

response of composite materials due to damage. The finite strain formulation further involves an a priori volumetric and distortional energy decomposition.

Demonstrations have been given in terms of numerical examples utilizing both synthetic and actual data in determining both the elastic and inelastic material parameters.

We are currently working in extending these energy formulations to approaches that achieve two main goals. First, focus on approaches that do not require FEA in the loop, and second, on approaches that incorporate the stochastic nature of the material response and the acquired data in a manner that quantifies uncertainty. This quantification should utilize prior knowledge via Bayesian based stochastic formalisms, which enable incremental and recursive algorithms based on Kalman filtering and in general, information theory.

Acknowledgment

The authors acknowledge the support by the Office of Naval Research and by NRL's 6.1 core-program. The authors also express their gratitude to Dr. Phillip Mast for providing us with pioneering inspiration by initiating both the dream and the reality of industrialized material characterization in the sixties and allowed us to stand on his giant shoulders.

References

[1] Kaczmar, J., Pietrzak, K., and Wlosinski, W., 2000, "The Production and Application of Metal Matrix Composite Materials," J. Mater. Process. Technol., **106**(1–3), pp. 58–67.

[2] Baker, A., Dutton, S., and Kelly, D., 2004, "Composite Materials for Aircraft Structures," 2nd ed., AIAA, Reston, VA.

[3] Daniel, I., and Ishai, O., 1994, *Engineering Mechanics of Composite Materials*, Oxford University Press, New York.

[4] Carlsson, L., and Pipes, R., 1997, *Experimental Characterization of Advanced Composite Materials*, CRC Press, FL.

[5] Mast, P., Beaubien, L., Clifford, M., Mulville, D., Sutton, S., Thomas, R., Tirosh, J., and Wolock, I., 1983, "A Semi-Automated In-Plane Loader for Materials Testing," Exp. Mech., **23**(2), pp. 236–241.

[6] Mast, P., Nash, G., Michopoulos, J., Thomas, R., Badaliance, R., and Wolock, I., 1992, "Experimental De-Termination of Dissipated Energy Density as a Measure of Strain-Induced Damage in Composites," Technical Report Tec. Rpt. NRL/FR/6383–92–9369, Naval Research Laboratory, Washington, DC, USA.

[7] Mast, P., Nash, G., Michopoulos, J., Thomas, R., Badaliance, R., and Wolock, I., 1995, "Characterization of Strain-Induced Damage in Composites Based on the Dissipated Energy Density Part I. Basic Scheme and Formulation," Theor. Appl. Fract. Mech., **22**(2), pp. 71–96.

[8] Michopoulos, J., 2003, *Computational and Mechatronic Automation of Multiphysics Research for Structural and Material Systems*, Recent Advances in Composite Materials: In Honor of S. A. Paipetis, Kluwer Academic Press, pp. 9–21.

[9] Michopoulos, J., 2004, "Mechatronically Automated Characterization of Material Constitutive Response," *Proceedings of the 6th World Congress on Computational Mechanics (WCCM-VI)*, Tsinghua University Press and Springer, Beijing China, pp. 486–491.

[10] Michopoulos, J., Hermanson, J., and Furukawa, T., 2008, "Towards the Robotic Characterization of the Constitutive Response of Composite Materials," Compos. Struct., **86**(1–3), pp. 154–164.

[11] Michopoulos, J. G., Hermanson, J. C., and Iliopoulos, A. P., 2010, "Towards a Recursive Hexapod for the Multidimensional Mechanical Testing Of Composites," 2010 ASME International Design Engineering Technical Conferences & Computers and Information In Engineering Conference, August 15–18, 2010, Montreal, Quebec, Canada, Paper No. DETC2010/CIE–28699.

[12] Pierron, F., Vert, G., Burguete, R., Avril, S., Rotinat, R., and Wisnom, M., 2007, "Identification of the Orthotropic Elastic Stiffnesses of Composites With the Virtual Fields Method: Sensitivity Study and Experimental Validation," Strain, **43**(3), pp. 250–259.

[13] Cooreman, S., Lecompte, D., Sol, H., Vantomme, J., and Debruyne, D., 2007, "Elasto-Plastic Material Parameter Identification by Inverse Methods: Calculation of the Sensitivity Matrix," Int. J. Solids Struct., **44**(13), pp. 4329–4341.

[14] Furukawa, T., and Michopoulos, J., 2008, "Computational Design of Multiaxial Tests for Anisotropic Material Characterization," Int. J. Numer. Methods Eng., **74**(12), pp. 1872.

[15] Michopoulos, J., Iliopoulos, A., and Furukawa, T., 2009, "Accuracy of Inverse Composite Laminate Characterization Via the Mesh Free Random Grid Method," *Proceedings of the ASME 2009 International Design Engineering Technical Conferences & Computers and Information in Engineering Conference IDETC/CIE 2009*, ASME (ed.), Paper No. DETC2009/CIE–87096.

[16] Bruno, L., Furgiuele, F., Pagnotta, L., and Poggialini, A., 2002, "A Full-Field Approach for the Elastic Characterization of Anisotropic Materials," Opt. Lasers Eng., **37**(4), pp. 417–431.

[17] Schmidt, T., Tyson, J., and Galanulis, K., 2003, "Full-Field Dynamic Displacement and Strain Measurement Using Advanced 3D Image Correlation Photogrammetry: Part 1," Exp. Tech., **27**(3), pp. 47–50.

[18] Kajberg, J., and Lindkvist, G., 2004, "Characterisation of Materials Subjected to Large Strains by Inverse Modelling Based on In-Plane Displacement Fields," Int. J. Solids Struct., **41**(13), pp. 3439–3459.

[19] Meuwissen, M., Oomens, C., Baaijens, F., Petterson, R., and Janssen, J., 1998, "Determination of the Elastoplastic Properties of Aluminium Using a Mixed Numerical-Experimental Method," J. Mater. Process. Technol., **75**(1), pp. 204–211.

[20] Molimard, J., Le Riche, R., Vautrin, A., and Lee, J., 2005, "Identification of the Four Orthotropic Plate Stiffnesses Using a Single Open-Hole Tensile Test," Exp. Mech., **45**(5), pp. 404–411.

[21] Grediac, M., Toussaint, E., and Pierron, F., 2002, "Special Virtual Fields for the Direct Determination of Material Parameters With the Virtual Fields Method. 1-Principle and definition," Int. J. Solids Struct., **39**(10), pp. 2691–2705.

[22] Grediac, M., and Pierron, F., 2006, "Applying the Virtual Fields Method to the Identification of Elasto-Plastic Constitutive Parameters," Int. J. Plast., **22**(4), pp. 602–627.

[23] Chalal, H., Avril, S., Pierron, F., and Meraghni, F., 2006, "Experimental Identification of a Nonlinear Model for Composites Using the Grid Technique Coupled to the Virtual Fields Method," Composites Part A, **37**(2), pp. 315–325.

[24] Michopoulos, J., and Iliopoulos, A., 2009, "A Computational Workbench for Remote Full Field 2D Displacement and Strain Measurements," *Proceedings of the ASME 2009 International Design Engineering Technical Conferences & Computers and Information in Engineering Conference IDETC/CIE 2009*, ASME (ed.), Paper No. DETC2009/CIE–86900.

[25] Andrianopoulos, N., and Iliopoulos, A., 2006, "Displacements Measurement in Irregularly Bounded Plates Using Mesh Free Methods," *Fracture of Nano and Engineering Materials and Structures*, E. Gdoutos, ed., Springer, Dordrecht, pp. 587–588.

[26] Iliopoulos, A., Michopoulos, J., and Andrianopoulos, N., 2009, "Performance Sensitivity Analysis of the Mesh-Free Random Grid Method for Whole Field Strain Measurements," *Proceedings of the ASME 2008 International Design Engineering Technical Conferences & Computers and Information in Engineering Conference IDETC/CIE 2008*, Brooklyn, New York, pp. 545–555.

[27] Iliopoulos, A., and Michopoulos, J., 2009, "Sensitivity Analysis of the Mesh-Free Random Grid Method for Measuring Deformation Fields on Composites," *Proceedings of the 17th International Conference on Composite Materials, ICCM–17: 27 Jul 2009–31 Jul 2009*, The British Composites Society: Edinburgh International Convention Centre (EICC), Edinburgh, UK.

[28] Iliopoulos, A., and Michopoulos, J., 2009, "Effects of Anisotropy on the Performance Sensitivity of the Mesh Free Random Grid Method for Whole Field Strain Measurement," *Proceedings of the ASME 2009 International Design Engineering Technical Conferences & Computers and Information in Engineering Conference IDETC/CIE 2009*, ASME (ed.), Paper No. DETC2009/CIE–86962.

[29] Michopoulos, J., and Furukawa, T., 2007, "Multi-Level Coupling of Dynamic Data-Driven Experimentation With Material Identification," Lect. Notes Comput. Sci., **4487**, pp. 1180.

[30] Furukawa, T., Michopoulos, J., and Kelly, D., 2008, "Elastic Characterization of Laminated Composites Based on Multiaxial Tests," Compos. Struct., **86**(1–3), pp. 269–278.

[31] Furukawa, T., and Michopoulos, J., 2008, " Online Planning of Multiaxial Loading Paths for Elastic Material Identification," Comput. Methods Appl. Mech. Eng., **197**, pp. 885–901.

[32] Man, H., Furukawa, T., and Kellermann, D., 2008, "Implicit Constitutive Modeling Based on the Energy Principle," *Proceedings of XXII ICTAM, 25–59 August 2008*, Adelaide, Paper No: 11427.

[33] Michopoulos, J., Furukawa, T., and Lambrakos S., 2009, "Data-Driven Characterization of Composites Based on Virtual Deterministic and Noisy Multiaxial Data," 2008 ASME International Design Engineering Technical Conferences and omputers and Information in Engineering Conference, DETC 2008, Vol. **3**, New York City, NY, pp. 1095–1106.

[34] Furukawa, T., and Pan, J., 2009, "Stochastic Identification of Elastic Constants for Anisotropic Materials," Int. J. Numer. Methods Eng., **81**(4), pp. 429–452.

[35] Samarasinghe, S., 2006, "Neural Networks for Applied Sciences and Engineering," *From Fundamentals to Complex Pattern Recognition*, 1st ed., Auerbach Publications, Boston, MA.

[36] Michopoulos, J., 1992, "Constitutive Characterization of Composites Via Artificial Neural Nets," Code 6383 Internal Report, NRL April 1992.

[37] Leighton, R., 1994, "AspirinMIGRAINES," release v7.0.

[38] Yagawa, G., Yoshimura, S., Okuda, H., and Furukawa, T., 1996, "Innovative Approaches for Modelling of Inelastic Material Behaviors," *(Applications of Neural Networks and Evolutionary Algorithms), Localized Damage IV: Computer-Aided Assessment and Control*, pp. 169–184.

[39] Furukawa, T., and Yagawa, G., 1998, "Implicit Constitutive Modelling for Viscoplasticity Using Neural Networks," Int. J. Numer. Methods Eng., **43**, pp. 195–219.

[40] Furukawa, T., and Hoffman, M., 2004, "Accurate Cyclic Plastic Analysis Using a Neural Network Material Model," Eng. Anal. Boundary Elem., **28**(3), pp. 195–204.

[41] Man, H., Furukawa, T., Hoffman, M., Imlao, S., and Lou, Z. H., 2007, "An Indirect Implicit Model for Frequency Dependent Hystereses of Piezoelectric Ceramics," J. Aust. Ceram. Soc., **43**(2), pp. 169–174. See http://www.austceram.com/_data/docs/journal/jacs2007-2/jacs_2007_43_2_man%2815%29.pdf.

[42] Man, H., Furukawa, T., Hoffman, M., and Imlao, S., 2008, "An Indirect Implicit Technique for Modelling Piezoelectric Ceramics," Comput. Mater. Sci., **43**(4), pp. 629–640.

[43] Ghaboussi, J., and Sidarta, D., 1998, "New Nested Adaptive Neural Networks (NANN) for Constitutive Modeling," Comput. Geotech., **22**(1), pp. 29–52.

[44] Shin, H., and Pande, G., 2003, "Identification of Elastic Constants for Orthotropic Materials From a Structural Test," Comput. Geotech., **30**(7), pp. 571–577.

[45] Jung, S., and Ghaboussi, J., 2006, "Neural Network Constitutive Model for Rate-Dependent Materials," Comput. Struct., **84**(15–16), pp. 955–963.

[46] Haj-Ali, R., and Kim, H., 2007, "Nonlinear Constitutive Models for FRP Composites Using Artificial Neural Networks," Mech. Mater., **39**(12), pp. 1035–1042.

[47] Man, H., Furukawa, T., Herszberg, I., and Prusty, G., 2009, "Implicit Modeling of Damage Behavior for Composite Materials Using an Energy-Based Method," SAMPE '09 Spring Symposium Conference Proceedings, 18–21 May 2009, Baltimore, MD, pp. 54, Paper No. 5704.

[48] van Rietbergen, B., Odgaard, A., Kabel, J., and Huiskes, H. W. J., 1996, "Direct Mechanics Assessment of Elastic Symmetries and Properties of Trabecular Bone Architecture," J. Biomech., **29**, pp. 1653–1657.

[49] Neidinger, R. D., 1995, "Computing Multivariable Taylor Series to Arbitrary Order," APL95 Conference Proceedings, APL Quote Quad, **25**(4), pp. 134–144.

[50] Lawson, C. L., and Hanson, R. J., 1996, *Solving Least Squares Problems*, Prentice-Hall, Englewood Cliffs, NJ, 1974, Reprinted 1996 by SIAM Publications, Philadelphia, PA.

[51] Wolfram Research, Inc., 2008, Mathematica, Version 7.0, Champaign.

[52] Haupt, P., 2000, Continuum *Mechanics and Theory of Materials*, Springer-Verlag, Berlin Heidelberg.

[53] Matzenmiller, A., Lubliner, J., and Taylor, R. L., 1995, "A Constitutive Model for Anisotropic Damage in Fiber—Composites," Mech. Mater., **20**, pp. 125–152.

[54] Van Der Meer, F. P., Sluys, L. J., 2009, "Continuum Models for the Analysis of Progressive Failure in Composite Laminates," J. Compos. Mater., **43**(20), pp. 2131–2156.

[55] Voyiadjis, G. Z., Ju, J. W., and Chaboche, J.-L., 1998, *Damage Mechanics in Engineering Materials*, Elsevier Science, Amsterdam.

[56] Kaliske, M., 2000, "A Formulation of Elasticity and Viscoelasticiy for Fibre Reinforced Material at Small and Finite Strains," Comput. Methods Appl. Mech. Eng., **85**, pp. 225–243.

[57] Ryan, K. F., 1990, "Dynamic Response of Graphite/Epoxy Plates Subjected to Impact Loading," MSc thesis, MIT, Cambridge, MA.

[58] Wegner, P. M., and Adams, D. F., 2000, "Verification of the Combined Load Compression (CLC) Test Method," DOT/FAA Technical Report DOT/FAA/AR–00/26.

[59] Vaidya, R. S., and Sun, C. T., 1997, "Fracture Criterion for Notched Thin Composite Laminates," AIAA J., **35**(2), pp. 311–314.

[60] Minguet, P. J., Dugundji, J., and Lagace, P. A., 1989, "Postbuckling Behavior of Laminated Plates Using a Direct Energy-Minimization Technique," AIAA J., **27**(12), pp. 1785–1792.

[61] Lessard, L. B., Eilers, O. P., and Shokrieh, M. M., 1995, "Testing of In-plane Shear Properties Under Fatigue Loading," J. Compos. Reinf. Plast., **14**(9), pp. 965–987.

[62] Esp, B., Chan, W. S., 2008, "Two Parameter Approximation to the Orthotropic Stress Concentration Factor," SAMPE 2008—Long Beach, CA, May 18–22.

[63] Jones, D. R., Perttunen, C. D., Stuckman, B. E., 1993, "Lipschitzian Optimization Without the Lipschitz Constant," J. Optim. Theory Appl., **79**, pp. 157.

[64] The Mathworks, "Matlab," http://www.mathworks.com

[65] Spall, J. C., 2003, *Introduction to Stochastic Search and Optimization*, Wiley, NJ.

[66] ANSYS, Inc., 2009, ANSYS® Mechanical, Release 11.0.